EurJIC European Journal of Inorganic Chemistry

ChemPubSoc Europe

FULL PAPER

DOI:10.1002/ejic.201201077

Theoretical Perspectives on Redox "Non-Innocent" Oxazolidine *N*-Oxide Iron Nitroxide Complexes

CLUSTER ISSUE

Subrata Tewary,[a] Ian A. Gass,[b] Keith S. Murray,*[b] and Gopalan Rajaraman*[a]

Keywords: Radicals / Iron / Density functional calculations / Spin crossover / Magnetic properties

One-electron redox processes in ligands that exhibit non-innocent behaviour invariably leads to the generation of radical species, which, when coupled with redox-active metal centres, can lead to strong magnetic exchange, ambiguous electronic structures and even spin crossover (SCO). We have chosen two iron complexes $[Fe^{II}(\mathbf{L}^{\cdot})_2](BF_4)_2$ (**1**) and $[Fe^{III}(\mathbf{L}^{-})_2](BPh_4)$ (**2**) [with $\mathbf{L}^{\cdot}$ = 4-dimethyl-2,2-di(2-pyridyl)oxazolidine *N*-oxide] as the basis for an extensive theoretical study to determine the influence and interplay of the strong magnetic exchange, the redox non-innocent behaviour and any possible spin transitions. A series of calculations established the low-spin character of the Fe in both the complexes and gave us valuable insight into the electronic structure of **1** and **2** along with their one- and two-electron reduced species. An attempt has been made to relate the bonding features to the energy difference between different spin states and to the influence of the exchange coupling on any possible SCO properties.

Introduction

There is a great deal of interest in the synthesis and study of nitroxide radicals owing to their kinetic stability under ambient conditions,[1] which has led to the use of various analytical/spectroscopic techniques such as electron paramagnetic resonance (EPR) spectroscopy to probe their electronic structure. The unpaired electron on the nitroxides has led to their use as spin probes,[2] organic ferromagnetic materials[3–6] and as bridging ligands for paramagnetic metal ions.[1] Meanwhile, discrete metal–radical complexes with a well-defined geometry are good candidates for fundamental studies on magneto-structural correlations. Such investigation is necessary not only for understanding the magnetic-exchange mechanism between the metal and organic radical but also for guiding the design of new organic radical ligands for the development of novel molecular magnetic materials. On many occasions, the weakly basic nitroxides have been combined with strongly ligating sites like pyridine,[7] pyrazines,[8] 2,2′-bipyridine[9] and imidazoles[10] to make the radical coordinate effectively with the metal ions.

A molecular orbital (MO) approach is necessary to understand the bonding of such radicals with a metal ion.[11] The unpaired electron of nitroxide radicals is in a π* orbital, which is equally localised over the nitroxide N–O moiety. When the nitroxide radical binds to a metal ion, it usually coordinates through the terminal oxygen leading to two possible cases that might arise from this situation. The first involves a positive overlap between the metal orbital(s) that contain the unpaired electron(s) and the nitroxide radical, which might form a strong covalent bond and therefore an antiferromagnetic interaction. In the second case, if the metal orbitals that contain the unpaired electrons are orthogonal to the radical, it gives rise to ferromagnetic exchange between the magnetic orbitals and the radical spin. Simple nitroxides such as NITR[1] (2-R-4,4,5,5-tetramethyl-4,5-dihydro-1*H*-imidazol-1-oxyl-3-oxide, with R = methyl, ethyl, propyl, and phenyl) can bind to a metal ion axially or equatorially, usually in tandem with electron-withdrawing groups such as hexafluoroacetylacetonato (hfac) to lead to up to two nitroxide radicals coordinated either in the axial or equatorial position. In the case of Cu^{II}–radical complexes, the observation of ferro-[12–14] and antiferromagnetic[11,15,16] interactions was rationalised by means of such axial or equatorial coordination, respectively.

Synthesis of metal dimers by using nitroxide radicals is a very diverse field and many complexes have been synthesised to develop ferromagnetic or ferrimagnetic types of interactions.[1] The use of organic spin carriers in conjunction with paramagnetic metal ions as building blocks to develop novel magnetic materials has been labelled the "metal–radical approach" and was pioneered by Gatteschi and co-workers with the use of nitroxide radicals.[11] The very first example of a molecular-based ferromagnet was an Fe–radical system in which the tetracyanoethylenide (tcne) radical

[a] Department of Chemistry,
Indian Institute of Technology Bombay,
Powai, Mumbai, 400076, India
E-mail: rajaraman@chem.iitb.ac.in
Homepage: http://www.chem.iitb.ac.in/~rajaraman/
[b] School of Chemistry Monash University,
Clayton, Victoria 3800, Australia
E-mail: keith.murray@monash.edu
Homepage: http://monash.edu/science/about/schools/chemistry/staff/murray.html

anion is coordinated to an Fe ion to form the charge-transfer complex $[Fe(\eta_5\text{-}C_5Me_5)_2]^{\cdot+}[tcne]^{\cdot-}$.[17]

The $[Fe^{III}(rad)(mnt)_2]$ (rad^+ = 2-(*para*-*N*-methylpyridinium)-4,4,5,5-tetramethylimidazoline-1-oxyl, mnt^{2-} = *cis*-1,2-dicyano-1,2-ethylenedithiolato) complex reported by Kahn et al. has an apically bound nitroxide that forms a square-pyramidal $Fe^{III}(S_4O)$ complex that exhibits both simultaneous magnetic exchange and an $S = 3/2$ to $S = 1/2$ spin crossover.[18] This piqued our interest in studying the effects of exchange and spin crossover in Fe^{II} nitroxides. The paucity of low-spin Fe^{II} radical species,[19–21] the propensity of Fe^{II} to undergo a spin transition and the redox-active nitroxide ligands suggest that such Fe^{II} nitroxides are ideal model complexes for further study. Such complexes could conceivably offer strong magnetic exchange, non-innocent behaviour and the possibility of spin crossover all occurring simultaneously in a single molecule. In this regard, the recently reported congeners $[Fe^{II}(\mathbf{L}^{\cdot})_2](BF_4)_2$ (**1**) and $[Fe^{III}(\mathbf{L}^{\cdot})_2](BPh_4)$ (**2**) in which $\mathbf{L}^{\cdot}$ = 4-dimethyl-2,2-di(2-pyridyl)oxazolidine *N*-oxide have been chosen for further theoretical treatment.[22] Two ligands, each of which contain one nitroxide radical that coordinates axially and two equatorially coordinated pyridyl groups, form in a bis-terdentate fashion around the central Fe ion. The dication $[Fe^{II}(\mathbf{L}^{\cdot})_2]^{2+}$ in **1** undergoes a one-electron reduction to the intermediate $[Fe^{II}(\mathbf{L}^{\cdot})(\mathbf{L}^{-})]^{+}$, which then undergoes an intramolecular electron transfer to generate the $[Fe^{III}(\mathbf{L}^{-})_2]^{+}$ monocation found in **2**. The ligand is in the neutral radical form in **1** and in the hydroxylamino anionic form in **2** with both Fe ions in the low-spin state. Complex **2** is formed by a reductively induced oxidation of the central iron ion. In addition to this interesting redox behaviour, complex **1** has a linear $\mathbf{L}^{\cdot}$–Fe^{II}–$\mathbf{L}^{\cdot}$ arrangement, which offers a unique model system to examine the radical–radical exchange by means of the low-spin Fe^{II} ion.

By using density functional methods, we have attempted to understand more fully the electronic structure, magnetic exchange, redox behaviour and the possibility of spin crossover of complexes **1** and **2** by computing structural, energetic and spectroscopic parameters.

Computational Details

X-ray structural parameters have been taken as an initial starting point for all the calculations. Two software suites, namely, Gaussian 09[23] and ORCA,[24] have been used for computing structure and spectroscopic parameters such as *g* tensors, Mössbauer isomer shifts (IS) and quadrupole splittings (QS). We have used the broken-symmetry approach developed by Ginsberg and Noodleman et al.,[25] which has been proven to give a good estimate of the exchange coupling constant. Details regarding the evaluation of *J* values using the broken-symmetry approach for dinuclear as well as polynuclear complexes can be found elsewhere.[26–29] Geometry optimisations and single-point calculations have been performed by using the B3LYP[30,31] functional. For all calculations, we have used the triple-ζ valence (TZV)[34] basis set of Ahlrichs and co-workers[32,33] for all the elements. Geometry optimisation and frequency calculations were performed to confirm the minima in the potential-energy surface that yields the enthalpy and entropy for different species. The enthalpy and entropy values are estimated from the vibrational contributions. For calculating *g*-tensor components, the B3LYP functional has been used along with the triple-ζ valence basis set as described above by considering a significant polarisation to all the atoms. The EPR properties were predicted by coupled perturbed Kohn–Sham theory along with the spin–orbit mean-field method developed by Neese et al.[35] For the Mössbauer IS and QS parameters we relied on the pure BP86 functional,[36] as this has been shown to yield better estimations than experiments.[37] The relativistic effects were incorporated by using the ZORA[38,39] method implemented in ORCA along with the RIJCOSX approximation to accelerate the process of calculation. The spin states are represented by the following notation: $^{M}\mathbf{1}_{\text{spin state}}$, whereby superscript "M" denotes the total multiplicities ($2S + 1$) of the complexes and subscript "spin state" denotes the spin state LS (low spin), HS (high spin) or IS (intermediate spin) on the Fe^{II} atoms, with the numeral **1** denoting the species.

In addition, a limited method assessment has been carried out to cross-check the reliability of the B3LYP functional, and here we have performed geometry optimisation of selected spin states with functionals such as BP86,[36] BLYP,[40] OLYP,[43] B3LYP*[44] and the M06-2X[41] suite. The initial section addresses the performance of different functionals in the estimation of structure and properties of these complexes. Some low-lying configurations have been calculated by incorporating solvent effects to check the role of solvation on the different electronic states of the metal ion and the radicals. Acetonitrile is used as the solvent because it was used in the synthesis of these complexes.[22] The polarisable continuum model (PCM)[45] with Onsager's SCRF code, which is further extended by Wiberg and co-workers[46] for Gaussian, have been employed for solvation calculations.[47] This is a continuum solvation model that is based on the multipole expansion (MPE)[48] of the solute charge distribution.

Results and Discussion

Complexes **1** and **2**[22] differ only in the physical oxidation state of the metal ions, the type and number of anions and the nature of the ligand. In **1**, the ligand exists in the neutral radical form ($\mathbf{L}^{\cdot}$), whereas in **2** it exists in the hydroxylamino anionic form ($\mathbf{L}^{-}$). Nitroxide N–O bond lengths from X-ray structural studies are useful in assigning the nature of the nitroxide ligand. For example, free-radical ligands such as Proxyl (2,2,5,5-tetramethylpyrrolinyl-1-oxyl), Tempo (2,2,6,6-tetramethylpiperidin-1-yl)oxyl or NITR have N–O bond lengths in the range 1.27–1.28 Å.[1] In complex **1**, the N–O bond length is 1.317 Å, which is consistent with the neutral radical form ($\mathbf{L}^{\cdot}$), whereas in **2** it is 1.411 Å, which is indicative of the hydroxylamino an-

ionic form ($\mathbf{L}^{-}$). This can be rationalised when we consider that the extra electron in the hydroxylamino anionic form of the ligand is located in the antibonding π^* orbital, thereby resulting in a decrease in the N–O bond order and an overall bond lengthening.

The radical-ligand character and the metal oxidation states were established by using spectroscopic, electrochemical, magnetic, structural and theoretical studies.[22] For complex **1**, the $S = 0$ ground state was determined from variable-temperature magnetic susceptibility measurements, structural studies and EPR spectroscopy. Mössbauer spectroscopic studies established the low-spin (LS) Fe^{II} configuration. The magnetic data were fitted by using a strong antiferromagnetic exchange interaction between the two radical centres through the LS Fe^{II} centre, and this yields a J value of –315 cm^{-1}. For **2**, a $S = 1/2$ ground state was unambiguously established by using magnetic susceptibility measurements, EPR and Mössbauer spectroscopy, thereby resulting in an LS Fe^{III} configuration. Electrochemical studies resulted in square reaction schemes that show the redox intermediates involved and the reversible redox behaviour of complexes **1** and **2**. Preliminary DFT calculations supported the diamagnetic ground state for **1** and $S = 1/2$ ground state for complex **2**.

Role of Exchange-Correlation Functionals in Predicting the Ground State of 1

DFT calculations of metal–radical systems are challenging tasks because the prediction of spin densities, and the estimation of spin-state energies and exchange parameters require an accurate description of electron correlation effects.[49] Within DFT formalism, this is often done by parameterising the functional to suit the specific system of interest. A similar approach has been performed to estimate accurate spin-density values for Cu^{II} complexes.[50] In our systems of interest, one of the major hurdles with the B3LYP functional is that it predicts a ferromagnetic coupling between two radical centers with LS Fe^{II} configuration, while experiments suggest that the interaction is antiferromagnetic (see below). Thus we have decided to carry out a limited method assessment to check the reliability of other functionals. We performed additional calculations by employing pure functionals such as BP86,[36] BLYP[40] and OLYP,[43] along with the hybrid functional B3LYP*, which possesses 15% HF exact exchange.[44] Also a check has been made with the modern *meta*-GGA M06-2X[41] functional, which possesses a large amount of HF exchange. The OLYP functional led to a J value of –259.5 cm^{-1}, and this was found to be the closest to the experimental values among the tested functionals. The BLYP functional yields a J value of –408.7 cm^{-1}, whereas BP86 yields a J value of –384.0 cm^{-1}. In the case of the B3LYP* functional, the estimated exchange constant (J) was found to be +99.5 cm^{-1}, whereas M06-2X also yields a ferromagnetic coupling with a J value of +37.9 cm^{-1}. The collected results are clearly divided, with pure functionals predicting antiferromagentic exchange with a marginal difference in the range of 55.5–93.7 cm^{-1} relative to experimental results. On the other hand, the B3LYP* functional yielded the ferromagnetic exchange, although the estimate is diminished by 44.4 cm^{-1} relative to the original B3LYP results. Hence it is very clear from the obtained result that the J value decreases as the HF exchange decreases, with the pure GGA functional able to predict the correct ground state for complex **1**.

Computed spin-density values for different functionals are given in Table 1 along with computed structural parameters in Tables 2 and 3. Hybrid functionals predict a small amount of spin density on Fe, whereas pure functionals predict a larger spin density on Fe than the radical atoms (more delocalisation). Computed structural parameters in comparison to X-ray structural values reveal that for the $^1\mathbf{1}_{LS}$ species of BLYP, OLYP and BP86 functionals, structures are calculated that are in good agreement with the X-

Table 1. Calculated spin densities of selected atoms of $^1\mathbf{1}_{LS}$ and $^3\mathbf{1}_{LS}$ spin states for complex **1** using B3LYP, B3LYP*, BLYP, OLYP, BP86 and M06-2X functionals.

	B3LYP		B3LYP*		BLYP		OLYP		BP86		M06-2X	
	$^3\mathbf{1}_{LS}$	$^1\mathbf{1}_{LS}$	$^3\mathbf{1}_{LS}$	$^1\mathbf{1}_{LS}$	$^3\mathbf{1}_{LS}$	$^1\mathbf{1}_{LS}$	$^3\mathbf{1}_{LS}$	$^1\mathbf{1}_{LS}$	$^3\mathbf{1}_{LS}$	$^1\mathbf{1}_{LS}$	$^3\mathbf{1}_{LS}$	$^1\mathbf{1}_{LS}$
Fe	0.208	0.0	0.309	0.0	0.552	0.0	0.463	0.0	0.486	0.0	0.016	0.0
O1	0.402	0.412	0.382	0.393	0.321	0.256	0.349	0.316	0.337	0.277	0.454	0.452
N1	0.492	0.503	0.461	0.471	0.381	0.288	0.428	0.369	0.411	0.322	0.528	0.531
O2	0.402	–0.412	0.382	–0.382	0.321	–0.256	0.349	–0.316	0.337	–0.277	0.454	–0.452
N2	0.492	–0.503	0.461	–0.461	0.481	–0.288	0.428	–0.369	0.411	–0.322	0.528	–0.531

Table 2. Selected structural parameters computed for the $^1\mathbf{1}_{LS}$ and $^3\mathbf{1}_{LS}$ spin states of complex **1** using B3LYP*, BLYP, OLYP, BP86 and M06-2X functionals. See Table 3 for B3LYP results.

	X-ray structure	B3LYP*		BLYP		OLYP		BP86		M06-2X	
		$^3\mathbf{1}_{LS}$	$^1\mathbf{1}_{LS}$	$^3\mathbf{1}_{LS}$	$^1\mathbf{1}_{LS}$	$^3\mathbf{1}_{LS}$	$^1\mathbf{1}_{LS}$	$^3\mathbf{1}_{LS}$	$^1\mathbf{1}_{LS}$	$^3\mathbf{1}_{LS}$	$^1\mathbf{1}_{LS}$
Fe–O	1.876	1.939	1.941	1.925	1.880	1.931	1.897	1.921	1.881	2.037	2.030
Fe–N1	1.973	2.016	2.014	2.014	2.023	2.013	2.018	1.992	1.998	2.056	2.053
Fe–N2	1.983	2.010	2.010	2.000	2.003	2.007	2.008	1.981	1.983	2.052	2.050
N–O	1.318	1.345	1.341	1.376	1.383	1.355	1.358	1.370	1.376	1.312	1.312
Fe–N–O	117.5	116.6	116.7	116.8	118.3	116.9	118.0	116.4	117.8	115.0	115.0

Table 3. Selected structural parameters obtained by experiment (X-ray) and B3LYP computed for species **1** and **2** for different spin configurations. Values given in parentheses are for complex **2**.

	X-ray structure	$^{1}\mathbf{1}_{LS}$	$^{3}\mathbf{1}_{LS}$	$^{1}\mathbf{1}_{IS}$	$^{3}\mathbf{1}_{IS}$	$^{5}\mathbf{1}_{IS}$	$^{3}\mathbf{1}_{HS}$	$^{5}\mathbf{1}_{HS}$	$^{7}\mathbf{1}_{HS}$	$^{2}\mathbf{1A}_{LS}$	$^{1}\mathbf{1B}_{LS}$	$^{5}\mathbf{1B}_{HS}$	$^{2}\mathbf{2}_{LS}$	$^{6}\mathbf{2}_{HS}$	$^{1}\mathbf{2A}_{LS}$	$^{1}\mathbf{2B}_{LS}$	$^{4}\mathbf{2B}_{LS}$
Fe–O	1.876 (1.859)	1.996	1.957	1.870	1.904	2.218	2.143	2.218	2.115	1.879	2.005	1.953	1.880	1.959	1.965	1.968	1.960
Fe–N1	1.973 (1.957)	2.021	2.022	2.006	1.996	2.033	2.205	2.032	2.197	1.992	1.965	2.284	1.991	2.175	2.021	2.021	2.011
Fe–N2	1.983 (1.982)	2.023	2.024	2.031	2.024	2.058	2.202	2.058	2.199	2.034	2.008	2.028	2.034	2.209	2.023	2.020	2.013
N–O	1.318 (1.412)	1.332	1.336	1.379	1.396	1.324	1.321	1.324	1.327	1.444	1.457	1.449	1.444	1.426	1.333	1.336	1.331
Fe–N–O	117.5 (115.9)	116.4	116.5	118.2	117.3	114.0	116.0	114.1	118.0	116.3	112.1	114.1	116.2	118.7	116.4	116.9	117.7

ray crystal structure, whereas structural parameters predicted by B3LYP, B3LYP* and M06-2X are in general slightly overestimated relative to X-ray structural parameters.

These results are similar to the finding of Kepp et al.[51] in which exchange-correlation functionals that possess approximately 10% HF exchange are found to be superior to B3LYP. Besides the above-mentioned functional, double-hybrid functionals such as B2PLYP have also been advocated for such classes of compounds.[52,53] Although B3LYP favours the HS state for complex **1**, the structure and properties computed using this functional are in reasonable agreement with the experimental results (see below). Thus calculations herein have been performed with the B3LYP functional and computations on other functionals are also performed wherever necessary to compare the computed B3LYP results with the experimental observation.

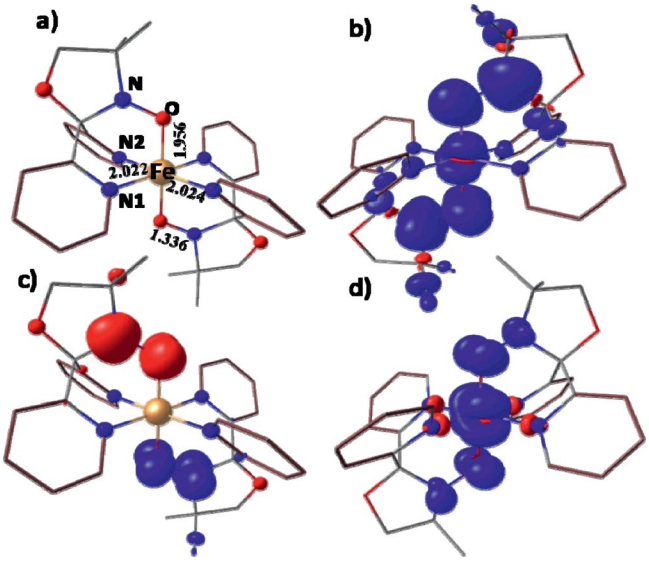

Figure 1. (a) B3LYP-optimised structure of **1** and computed spin-density plot for (b) $^{3}\mathbf{1}_{LS}$, (c) $^{1}\mathbf{1}_{LS}$ and (d) $^{2}\mathbf{2}_{LS}$.

Energetics and Structure

The B3LYP-optimised structure of **1** is given in Figure 1. For complex **1**, eight different spin configurations (see Table 4 for MO configurations) were computed that comprised the different spin states of Fe^{II}, namely, LS, IS and HS along with the possibility of ferromagnetic or antiferromagnetic exchange between the two radical centres. The Fe–O and the N–O experimental bond lengths vary for **1** and **2**, with **1** having longer Fe–O and Fe–N bond lengths as well as shorter N–O bond lengths than **2** (Table 3 and Table S1 in the Supporting Information). The longer N–O bond lengths in **2** are associated with the anionic character of the ligands, which leads to an increase in π(N–O)* character and hence a decrease in the bond lengths. Calculated bond lengths for different configurations can be found in Table 3. These computed bond lengths show longer bond lengths for the HS configurations than the experimental; as expected, a Jahn–Teller axial elongation for $^{5}\mathbf{1}_{IS}$ with equatorially elongated bond lengths was found for the $^{3}\mathbf{1}_{IS}$ and $^{1}\mathbf{1}_{IS}$ configurations. The LS configurations are consistent with the experimental values, the only significant deviation being larger Fe–O bond lengths. It is worth noting that the experimental data support the assignment of the $^{1}\mathbf{1}_{LS}$ configuration.

The computed energies are summarised in Table 4. Among the eight computed configurations, $^{7}\mathbf{1}_{HS}$ (HS Fe^{II} with radical coupled ferromagnetically; $S = 3$) is estimated

Table 4. Computed electronic configurations for **1** along with MO notation, gas-phase and solution-phase energy differences (ΔE_{sol}) corresponding to the ground state, enthalpy of change and entropy change in the gas phase. The energies and the ΔH are given in kJ mol^{-1}.

	MO notation	ΔE_{gas}	ΔE_{sol}	ΔH	ΔS [J mol^{-1} K^{-1}]
$^{3}\mathbf{1}_{LS}$	$\pi^{*}_{NO(1)}d_{x2-y2}\,d_{z2}\,d_{xy}\,d_{xz}\,d_{yz}\,\pi^{*}_{NO(2)}$	1.0	0.0	–2.1	8.8
$^{1}\mathbf{1}_{LS}$	$\pi^{*}_{NO(1)}\,d_{x2-y2}\,d_{z2}\,d_{xy}\,d_{xz}\,d_{yz}\,\pi^{*}_{NO(2)}$	3.2	2.2	0.0	0.0
$^{5}\mathbf{1}_{IS}$	$\pi^{*}_{NO(1)}d_{x2-y2}\,d_{z2}\,d_{xy}\,d_{xz}\,d_{yz}\,\pi^{*}_{NO(2)}$	39.7	64.1	34.0	44.5
$^{1}\mathbf{1}_{IS}$	$\pi^{*}_{NO(1)}d_{x2-y2}\,d_{z2}\,d_{xy}\,d_{xz}\,d_{yz}\,\pi^{*}_{NO(2)}$	59.4	58.9	59.3	24.8
$^{3}\mathbf{1}_{IS}$	$\pi^{*}_{NO(1)}d_{x2-y2}\,d_{z2}\,d_{xy}\,d_{xz}\,d_{yz}\,\pi^{*}_{NO(2)}$	89.0	–	78.1	27.3
$^{7}\mathbf{1}_{HS}$	$\pi^{*}_{NO(1)}d_{x2-y2}\,d_{z2}\,d_{xy}\,d_{xz}\,d_{yz}\,\pi^{*}_{NO(2)}$	0.0	7.3	–7.7	62.2
$^{5}\mathbf{1}_{HS}$	$\pi^{*}_{NO(1)}d_{x2-y2}\,d_{z2}\,d_{xy}\,d_{xz}\,d_{yz}\,\pi^{*}_{NO(2)}$	39.5	–	34.4	37.8
$^{3}\mathbf{1}_{HS}$	$\pi^{*}_{NO(1)}d_{x2-y2}\,d_{z2}\,d_{xy}\,d_{xz}\,d_{yz}\,\pi^{*}_{NO(2)}$	6.7	–	–0.9	59.2

to be lowest in energy (see ΔE_{gas} in Table 4), whereas the $^{1}\mathbf{1}_{LS}$ configuration (LS Fe^{II} radicals coupled antiferromagnetically) is 3.2 kJ mol^{-1} higher in energy. Solvation effects are expected to play an important role in influencing the energetics for Fe complexes.[54] Therefore we have optimised selected low-lying configurations by employing acetonitrile as the solvent. The solvation energetics (see ΔE_{sol} in

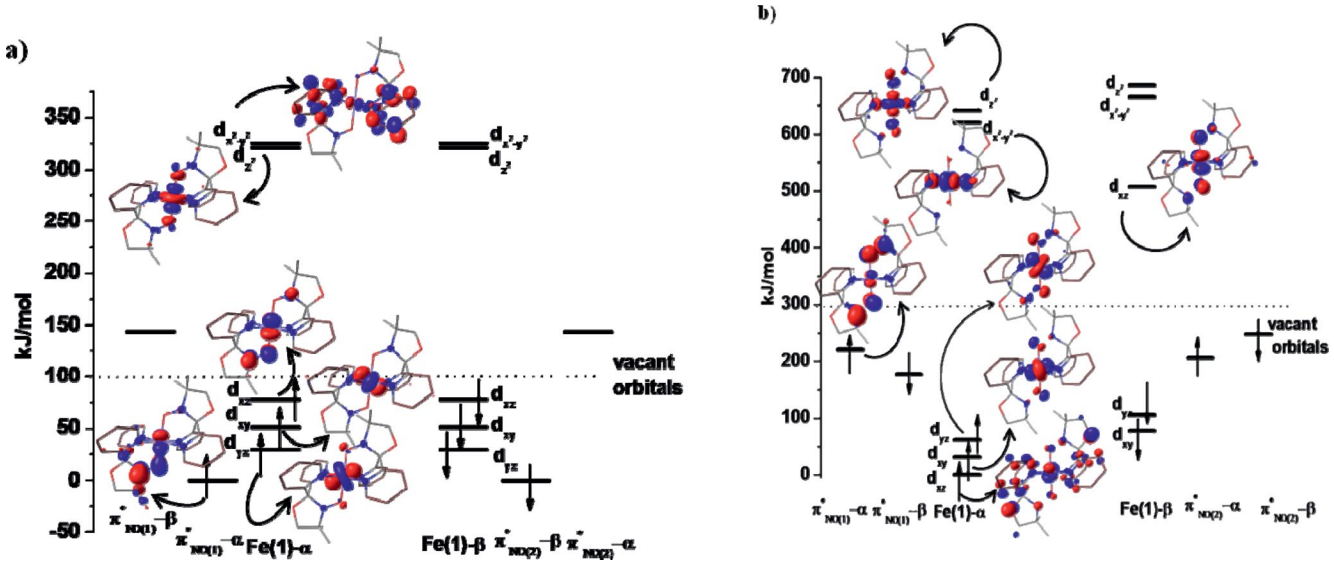

Figure 2. Eigenvalues plots for complex (a) **1** and (b) **2** computed using B3LYP.

Table 4) reveal that $^3\mathbf{1}_{LS}$ is the ground state with $^1\mathbf{1}_{LS}$ being only 2.2 kJ mol^{-1} higher in energy. The next configuration closest in energy is $^7\mathbf{1}_{HS}$, which is 7.3 kJ mol^{-1} higher in energy than $^3\mathbf{1}_{LS}$. Although the computed spin state of iron (Fe^{II} LS) is consistent with the experimental observations, our B3LYP predicts that the triplet is the ground state and this is in sharp contrast to the experimental observation of a diamagnetic ground state (see below). Experimental observation confirms that the ground state is a singlet, and here there are two possibilities to achieve a singlet state, one in the configuration $^1\mathbf{1}_{LS}$, in which it arises owing to antiferromagnetic interactions between the two radical centres, across LS Fe^{II}, and the second is the $^1\mathbf{1}_{IS}$ configuration, in which it arises owing to antiferromagnetic interaction between the intermediate spin (S = 1) Fe^{II} and the radical centres. However, our energetics reveal that the $^1\mathbf{1}_{IS}$ state is high-lying relative to $^1\mathbf{1}_{LS}$ by a margin of 58.9 kJ mol^{-1} and thus this state is unlikely to be the ground state for **1**. The experimental data support the $^1\mathbf{1}_{LS}$ configuration, which is calculated to be low-lying and close to the triplet ground state ($^3\mathbf{1}_{LS}$) with the high-spin configuration $^7\mathbf{1}_{HS}$ lying only 5.1 kJ mol^{-1} above. Interestingly, this suggests that there are LS and HS configurations with ferromagnetic coupling relatively close to the experimentally derived ground state.

For complex **2**, the $^2\mathbf{2}_{LS}$ configuration (LS Fe^{III}, S = 1/2) is found to be the ground state with the IS and HS configurations lying higher at 122.1 and 165.6 kJ mol^{-1}, respectively, in the gas phase. These excited states are very high-lying, and thus we expect this $^2\mathbf{2}_{LS}$ configuration to behave as a typical LS Fe^{III} ion that matches the experimental observations.

The eigenvalue plot for $^1\mathbf{1}_{LS}$ and $^2\mathbf{2}_{LS}$ along with MO plots are given in Figure 2. The unpaired electron on the radical centres are located in the π* orbitals, which are found to have a lateral π interaction with the d_{xz} orbital of the metal ion (see Figure 2). This strong π interaction is the probable cause of the large antiferromagnetic interaction between the two radical centres (see below). For complex **2**, upon reduction each π^*_{NO} orbital gains an electron, thus leading to the anionic form of the ligand, $\mathbf{L}^-$. The unpaired electron in **2** is found to be in the d_{xz} orbital. Since the d_{xz} orbital is also involved in strong π-bonding interaction with the ligand (see Figure 2), this suggests a charge-transfer transition with such a strong interaction that it leads to ligand non-innocent behaviour. The spin-density plot for $^3\mathbf{1}_{LS}$, $^1\mathbf{1}_{LS}$ and $^2\mathbf{2}_{LS}$ are shown in Figure 1b, c and d.

Reduction and Spin-Crossover Features of 1 and 2

We have also computed the energies of one-electron-reduced {**1A**, $[Fe^{II}(L^{\cdot})(L^-)]^+$} and -oxidized {**2A**, $[Fe^{III}(L^{\cdot})(L^-)]^{2+}$} species along with the two-electron-reduced {**1B**, $[Fe^{II}(L^-)(L^-)]$} and -oxidized {**2B**, $[Fe^{III}(L^{\cdot})(L^{\cdot})]^{3+}$} species, and the overall energetics computed for these species are summarised schematically in Figure 3 (see Table 3 for selected structural parameters) using B3LYP. All four species have been experimentally generated by using electrochemical methods, and some of them were detected using EPR spectroscopy.[22] EPR and electrochemical studies indicate that **1** is in equilibrium with **2A** (i.e., one of the ligands accepts an electron from the metal ions, thus leading to oxidation of the metal centre and reduction of the ligand species). Our calculations support this claim because species **2A** is merely 1.6 kJ mol^{-1} higher in energy than **1**, which suggests that **1** and **2A** are nearly isoenergetic. Generation of **2A** from **1** involves electron transfer from the metal-based orbital to one of the ligand π* orbitals, and the energy difference between the Fe(β-d_{xz}) orbital and NO(β-π*) orbital (see Figure 2a) is relatively small. The significant π interaction described earlier favours this charge-transfer process.

The molar fraction of HS as a function of pressure and temperature $\gamma_{HS}(p,T)$ is routinely used as an order param-

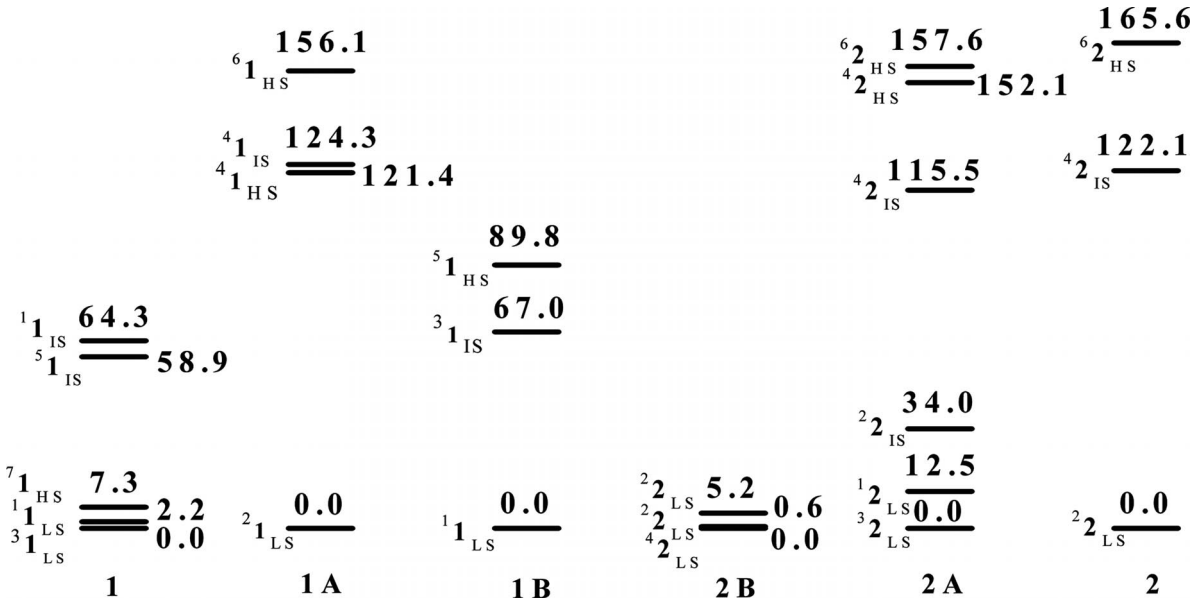

Figure 3. B3LYP-computed relative energies for different spin states for species **1**, **1A**, **1B**, **2**, **2A** and **2B**. All the energies are given in kJ mol^{-1} relative to the computed ground state of each species. For **1**, relative energies were given from the structural optimisation, whereas other energies reported are single-point energies computed on the X-ray structure.

eter for the spin transition and this is related to the free-energy difference $\Delta G(G_{HS} - G_{LS})$ by the following expression:[55]

$$\gamma_{HS} = \frac{1}{[1 + e^{(\Delta G/k_B T)}]}$$

At the transition temperature $T_{1/2}$, the equation can be approximated to the energy splitting between the HS and LS state (ΔE_s):[55]

$$T_{1/2} = \frac{\Delta E_s}{\Delta S_{1/2}}$$

ΔE_s is therefore the most important parameter in determining any possible SCO features.

For the six species **1**, **1A**, **1B**, **2**, **2A** and **2B** found in Figure 3, the ground state has an LS state for the Fe centre regardless of the oxidised or the reduced nature of the metal ion or ligand. A strong equatorial σ donation by the pyridine ligands and σ and π interaction by the axial oxygen atoms lead to a large energy gap between the t_{2g}-like and e_g-like orbitals in **1** and **2** (note that this gap is 242.7 kJ mol^{-1} for **1** and 558. 5 kJ mol^{-1} for **2**; see Figure 2). Looking at the electronic structures of **1** and **2**, it is apparent that (see Figure 2a) there is a strong π-bonding interaction between the Fe(d_{xz}) orbital and radical π orbitals. Complex **1** has the t_{2g}^6 ground-state configuration, so we would expect a π back-donation ($d_{xz} \rightarrow \pi^*$ radical), whereas for **2**, which has the t_{2g}^5 ground state and one hole in the β orbital of the Fe, both π donation and π back-donation are expected. This bonding picture is confirmed from the spin-density plots (Figure 1b–d).

It is to be noted here that a recent theoretical study indicates failure of most exchange-correlation functionals to reproduce correctly the spin densities of transition-metal complexes.[49] However, we believe that the relative trend observed in the spin density is still meaningful and can be used to understand the electronic structure of the complex of interest.[56] For complex **1**, the unpaired electrons are also found on the metal atom, particularly on the d_{xz} orbital, and this indicates that the donation of the β-electron from the β-π* orbital to the empty d_{xz} orbital is taking place. Similarly for complex **2**, the $\mathbf{L}^-$-character ligands also possess significant spin density, and this is essentially due to donation/back-donation between the Fe ion and radical ligands. Furthermore, for complex **1**, a large enthalpy change ($\Delta H = H_{LS} - H_{HS}$) and entropy contributions ($\Delta S = S_{LS} - S_{HS}$) are computed (see Table 4). This, along with large spin-state splitting between the LS and the IS and HS configurations (Figure 3), leads to the absence of any spin-crossover features in this series of complexes and this is consistent with the experimental observation.

Magnetic Exchange

The magnetic-exchange interaction has been calculated for species **1** and **2B** to understand the coupling between the two radical centres, which is mediated through the LS or Fe^{II} or Fe^{III} ions. For **1**, the Fe^{II} is in the LS configuration and there is only a single coupling between the two radical centres. The exchange Hamiltonian employed for complex **1** is given as

$$\hat{H} = -2J_1(\hat{S}_1 + \hat{S}_3)$$

for which S_1 and S_3 are the spins on the two radical centres ($S = 1/2$). This coupling is estimated to be ferromagnetic with a J value 143.9 cm^{-1} and this is contrary to the experimental estimate of –315 cm^{-1} but agrees with previous

B3LYP estimates.[22] Although deviation from experimental values for magnetic exchange is well known,[57,58] such a large deviation in sign and magnitude is unprecedented. It is to be noted here that the exchange interaction has been extracted experimentally by fitting the magnetic susceptibility plot in a way that assumes an interaction between the two $S = 1/2$ radical centres; however, there is an equilibrium process between species **1** and **2A** with around 5% of **2A** present in a sample of **1**. The small quantity of **2A** present (with a possible triplet ground state) cannot, however, solely account for the rise seen in the experimental $\chi_M T$ values, which is accounted for (in the majority) by the large radical–radical antiferromagnetic coupling, even at higher temperatures at which the magnetic moment would be expected to be influenced by **2A**. In **1**, there is a viable exchange pathway π*(NO)–d_{xz}(Fe)–π*(NO) and this π-type interaction will favour strong antiferromagnetic coupling. However, two other doubly occupied orbitals (d_{yz} and d_{xy}) are essentially orthogonal to the π*(NO) and thus lead to an overall ferromagnetic coupling.

For the HS configuration of **1** {HS $[Fe^{II}(L^{\cdot})_2]^{2+}$}, a different set of J values have been extracted. For HS Fe^{II} there are two J values (J_1 and J_2) assumed and the corresponding Hamiltonian is

$$\hat{H} = -2J_1(\hat{S}_1 \cdot \hat{S}_3) - 2J_2(\hat{S}_1 \cdot \hat{S}_2 + \hat{S}_2 \cdot \hat{S}_3)$$

in which S_1 and S_3 are the spin on two radical centres ($S = 1/2$) and S_2 is the spin on the HS Fe^{II} centre. The radical–radical J_1 interaction is estimated to be 901.2 cm^{-1}, whereas the J_2 exchange is 145.2 cm^{-1}. Both the exchanges are strong and are ferromagnetic in nature. For $\mathbf{1}_{IS}$, since some of the broken-symmetry solutions did not converge correctly, the exchange has not been computed.

For **2A**, $[Fe^{III}(L^{\cdot})(L^{-})]^{2+}$, the exchange between the Fe^{III} ion and radical system is estimated to be ferromagnetic with a J value of 524 cm^{-1}, whereas for $[Fe^{III}(L^{\cdot})(L^{\cdot})]^{3+}$ $\mathbf{2B}_{LS}$ the magnetic exchange values $J_1 = 81.2\ cm^{-1}$ and $J_2 = -12.9\ cm^{-1}$ and for $\mathbf{2B}_{HS}$ $J_1 = -17.8\ cm^{-1}$ and $J_2 = -367.7\ cm^{-1}$ are estimated. Interestingly, independent of the oxidation state of the Fe centre, the magnetic-exchange interactions are mostly ferromagnetic apart from the HS Fe^{III} case found in $\mathbf{2B}_{HS}$, in which the predominant exchange is antiferromagnetic in nature. The variation in the magnitude and sign of the exchange interactions over the various spin and oxidation states indicates a complex mechanism, which makes estimations of exchange interactions for the exchange-coupled, redox-active congeners studied here difficult.

Spin Hamiltonian Parameters

EPR g Tensor

The g tensor is an important quantity to check the presence of any radical system present. For complex **1**, temperature-dependent EPR experiments suggest that the ground state is a singlet but at higher temperatures a triplet-state signal is observed. The observed peaks in the EPR correspond to the contribution from **2A** {$[Fe^{III}(L^{\cdot})(L^{-})]^{2+}$}, which is in equilibrium with **1** and represents about 5% of the sample. We have carried out calculations to estimate the g-tensor components for species **2** in frozen solution in which the experimentally derived spectral parameters are $g_x = 2.163$, $g_y = 2.089$ and $g_z = 1.963$, whereas DFT yields values of $g_x = 2.091$, $g_y = 2.055$ and $g_z = 1.984$. Although the g tensors are underestimated relative to experiments, the rhombic nature of the g tensor predicted by experimental results is nicely reproduced in DFT. Underestimation of g-tensor values when using common exchange-correlation functionals is known and several methodologies including fine tuning of %HF exchange (one would require higher %HF here) can be employed to obtain good numerical estimates of g values.[50]

Mössbauer Parameters

Mössbauer spectroscopy is a valuable technique used to determine, unambiguously, the spin and oxidation states of Fe ions. There are two primary parameters that are important in Mössbauer spectroscopy, the isomer shift (IS) and the quadrupole splitting (QS). Both the parameters solely depend on the total electron density of the metal ion in question and not to the individual localised spin densities. Noodleman and co-workers have established a procedure of computing these parameters in transition-metal clusters.[59] The computed parameters for $^1\mathbf{1}_{LS}$, $^3\mathbf{1}_{LS}$ and $^2\mathbf{2}_{LS}$ are summarised in Table 5. In general, there is a good agreement between the experimental and calculated values, which adds support to the experimental interpretations. There is some deviation between the computed set and previously reported values[22] and this is essentially due to a slightly different basis set employed here.

Table 5. Mössbauer parameters computed by using BP86 functionals.

	Isomer shift IS [mm s^{-1}]		Quadrupole splitting QS [mm s^{-1}]	
	DFT	Exp. [78 K]	DFT	Exp. [78 K]
$^3\mathbf{1}_{LS}$	0.42	–	1.058	–
$^1\mathbf{1}_{LS}$	0.38	0.37	0.785	0.98
$^2\mathbf{2}_{LS}$	0.33	0.25	1.080	1.40

Conclusion

A theoretical study based on density functional methods has been undertaken to study the spin-state splitting, spin-coupling, spectral and possible SCO features of the Fe nitroxide systems reported recently.[22] Although the main focus is on **1** {$[Fe^{II}(L^{\cdot})_2](BF_4)_2$} and **2** {$[Fe^{III}(L^{-})_2](BF_4)$}, computational analysis has been performed on the one- and two-electron reduced species of **1** and **2** to gain a fuller understanding of the electronic structure of this Fe–radical system. The conclusions derived from this study are summarised below.

(i) Both species **1** and **2** possess the Fe atoms in LS configurations – a combination of multiple experimental techniques[22] is supported by our DFT calculations.

However, the hybrid functionals explored here, such as B3LYP, B3LYP* or M06-2X, are unable to reproduce the sign of the magnetic exchange correctly and this perhaps is due to overestimation of covalency.[50] On the other hand, pure functionals such as BP86, BLYP and OLYP reproduce the ground spin state and, with OLYP, the computed *J* values are found to be the closest to the experimental values.
(ii) Redox non-innocent behaviour proposed for these systems is independently verified by our calculations. Owing to very symmetric ligand arrangements and a significant interaction of the ligand NO π orbitals with the metal-based d orbitals, a non-innocent character for the ligand was detected whereby the donor/acceptor behaviour is determined by the electronic configuration of the metal centre. This behaviour is predicted by all the functionals tested.
(iii) A large splitting within the d orbitals was detected for species **1** as well as for **2**. The primary reason for the large ligand-field splitting observed is routed back to the Fe d_π–π*(NO) interaction between the metal and the ligand orbitals. This large splitting essentially leads to the absence of any SCO features because most of the SCO states are computed to be thermally inaccessible. A weaker π interaction with the metal d orbital is likely to help when observing the SCO features.
(iv) For species **1**, a ferromagnetic exchange computed by B3LYP is contrary to experimental results and the sign and strength of the magnetic exchange is found to strongly correlate to the Fe d-orbital configuration. This highlights the difficulty in estimating the exchange interaction in species in which spin transitions are expected/observed when hybrid functionals such as B3LYP or B3LYP* have been used. Pure functionals such as OLYP, BLYP or BP86, which possess a lower percentage of HF exchange, are perhaps better choices in this scenario.
(v) Computed *g* tensors and Mössbauer parameters confirm the LS nature of the Fe centres in species **1** and **2**, and computed values are generally in good agreement with the experimental observations.

In summary and in conjunction with the literature,[22] extensive theoretical studies have been undertaken to probe an Fe–radical system to underpin the electronic structure/non-innocent ligand behaviour and to relate the observed properties such as spin-coupling and SCO features. We predict that a moderate to weak π interaction of the radical with the metal d orbital, rather than the strong interaction noted here, is likely to yield SCO features in such systems.

Acknowledgments

K. S. M. and G. R. would like to acknowledge the financial support from the Indo-Australian Project (DST/INT/AUS/P-47/11) and generous computational resources from the Indian Institute of Technology-Bombay. S. T. thanks the University Grants Commission (UGC) for the JRF fellowship. Dr. W. D. Lupton is thanked for providing the organic radicals.

[1] A. Caneschi, D. Gatteschi, P. Rey, *Prog. Inorg. Chem.* **1991**, *39*, 331.
[2] a) L. J. Berliner (Ed.),*Spin Labelling Theory and Applications*, Academic Press, New York, **1976–1979**, vols. 1 and 2; b) J. F. W. Keana, *Chem. Rev.* **1978**, *78*, 37.
[3] M. Kinoshita, P. Turek, M. Tamura, K. Nozawa, D. Shiomi, Y. Nakazawa, M. Ichikawa, M. Takahashi, K. Awaga, T. Inabe, Y. Maruyama, *Chem. Lett.* **1991**, 1225.
[4] M. Takahashi, P. Turek, Y. Nakawaza, M. Tamura, K. Nozawa, D. Shiomi, M. Ishikawa, M. M. Kinoishita, *Phys. Rev. Lett.* **1991**, *67*, 746.
[5] T. Sugawara, M. M. Matsushita, A. Izuoka, N. Wada, N. Takeda, M. Ishikawa, *J. Chem. Soc., Chem. Commun.* **1994**, 1723.
[6] a) M. M. Matsushita, A. Izuoka, T. Sugawara, T. Kobayashi, N. Wada, N. Takeda, M. Ishikawa, *J. Am. Chem. Soc.* **1997**, *119*, 4369; b) D. Luneau, P. Rey, *Magnetism: A Supramolecular Function* (Ed.: O. Kahn), NATO ASI Series 484, Kluwer Academic Publishers, Dordrecht, The Netherlands, **1996**, p. 431.
[7] D. Luneau, F. M. Romero, R. Ziessel, *Inorg. Chem.* **1998**, *37*, 5078.
[8] a) D. Luneau, P. Rey, *Mol. Cryst. Liq. Cryst.* **1995**, *273*, 81; b) K. Fegy, T. Luneau, C. Ohm, P. Paulsen, P. Rey, *Angew. Chem.* **1998**, *110*, 1331; *Angew. Chem. Int. Ed.* **1998**, *37*, 1270.
[9] M. Nihei, T. Maeshima, Y. Kose, H. Oshio, *Polyhedron* **2007**, *26*, 1993.
[10] A. Caneschi, D. Gatteschi, A. Grand, J. Laugier, P. Rey, L. Pardi, *Inorg. Chem.* **1988**, *27*, 103.
[11] A. Caneschi, D. Gatteschi, R. Sessoli, P. Rey, *Acc. Chem. Res.* **1989**, *22*, 392.
[12] C. Benelli, D. Gatteschi, D. W. Carnegie Jr., R. L. Carlin, *J. Am. Chem. Soc.* **1985**, *107*, 2560.
[13] M. H. Dickman, R. J. Z. Doedens, *Inorg. Chem.* **1981**, *20*, 2677.
[14] L. C. Porter, M. H. Dickmann, R. J. Z. Doedens, *Inorg. Chem.* **1986**, *25*, 678.
[15] L. C. Porter, R. J. Doedens, *Inorg. Chem.* **1985**, *24*, 1006.
[16] Y. Y. Lim, R. S. Drago, *Inorg. Chem.* **1972**, *11*, 1334.
[17] J. S. Miller, J. C. Calabrese, A. J. Epstein, R. W. Bigelow, J. H. Zhang, W. M. J. Reiff, *Chem. Soc. Chem. Commun.* **1986**, 1026.
[18] J. P. Sutter, M. Fettouhi, L. Li, C. Michaut, L. Ouahab, O. Kahn, *Angew. Chem.* **1996**, *108*, 2250; *Angew. Chem. Int. Ed. Engl.* **1996**, *35*, 2113.
[19] D. Luneau, F. M. Romero, R. Ziessel, *Inorg. Chem.* **1998**, *37*, 5078.
[20] M. Nihei, T. Maeshima, Y. Kose, H. Oshio, *Polyhedron* **2007**, *26*, 1993.
[21] a) X. L. Wang, P. P. Yang, Z. W. Li, L. C. Li, D. Z. Liao, *Inorg. Chim. Acta* **2009**, *362*, 1901; b) P. Surawatanawong, S. Sproules, F. Neese, K. Wieghardt, *Inorg. Chem.* **2011**, *50*, 12064.
[22] I. A. Gass, J. C. Gartshore, W. D. Lupton, B. Moubaraki, A. Nafady, A. M. Bond, J. F. Boas, J. D. Cashion, C. Milsmann, K. Wieghardt, K. S. Murray, *Inorg. Chem.* **2011**, *50*, 3052.
[23] M. J. Frisch, G. W. Trucks, H. B. Schlegel, G. E. Scuseria, M. A. Robb, J. R. Cheeseman, G. Scalmani, V. Barone, B. Mennucci, G. A. Petersson, H. Nakatsuji, M. Caricato, X. Li, H. P. Hratchian, A. F. Izmaylov, J. Bloino, G. Zheng, J. L. Sonnenberg, M. Hada, M. Ehara, K. Toyota, R. Fukuda, J. Hasegawa, M. Ishida, T. Nakajima, Y. Honda, O. Kitao, H. Nakai, T. Vreven, J. A. Montgomery, Jr. J. E. Peralta, F. Ogliaro, M. Bearpark, J. J. Heyd, E. Brothers, K. N. Kudin, V. N. Staroverov, R. Kobayashi, J. Normand, K. Raghavachari, A. Rendell, J. C. Burant, S. S. Iyengar, J. Tomasi, M. Cossi, N. Rega, J. M. Millam, M. Klene, J. E. Knox, J. B. Cross, V. Bakken, C. Adamo, J. Jaramillo, R. Gomperts, R. E. Stratmann, O. Yazyev, A. J. Austin, R. Cammi, C. Pomelli, J. Ochterski, R. L. Martin, K. Morokuma, V. G. Zakrzewski, G. A. Voth, P. Salvador, J. J. Dannenberg, S. Dapprich, A. D. Daniels, O. Farkas, J. B. Foresman, J. V. Ortiz, J. Cioslowski, D. J. Fox, *Gaussian 09, Revision A.02*, Gaussian, Inc., Wallingford, CT, **2009**.
[24] F. Neese, *ORCA*, An ab initio, DFT and Semiempirical Electronic Structure Package, Version 2.7, Revision 0, Institut für Physikalische und Theoretische Chemie, Universität Bonn,

Bonn, Germany, **2010**; F. Neese, *Wiley Interdiscip. Rev.: Comput. Mol. Sci.* **2012**, *2*, 73.
[25] a) A. P. Ginsberg, *J. Am. Chem. Soc.* **1980**, *102*, 111; b) L. Noodleman, *J. Chem. Phys.* **1981**, *74*, 5737; c) L. Noodleman, C. Y. Peng, D. A. Case, J. M. Mouesca, *Coord. Chem. Rev.* **1995**, *144*, 199.
[26] E. Cremades, S. Gomez-Coca, D. Aravena, S. Alvarez, E. Ruiz, *J. Am. Chem. Soc.* **2012**, *134*, 10532.
[27] S. Gómez-Coca, E. Ruiz, *Dalton Trans.* **2012**, *41*, 2659.
[28] a) P. Comba, S. Hausberg, B. Martin, *J. Phys. Chem. A* **2009**, *113*, 6751; b) M. Atanasov, P. Comba, C. A. Daul, *Inorg. Chem.* **2008**, *47*, 2449; c) D. Reinen, M. Atanasov, *Springer Ser. Chem. Phys.* **2008**, *97*, 451.
[29] G. Rajaraman, F. Totti, A. Bencini, A. Caneschi, R. Sessoli, D. Gatteschi, *Dalton Trans.* **2009**, 3153.
[30] J. P. Perdew, *Phys. Rev. B* **1986**, *33*, 8822.
[31] A. D. Becke, *J. Chem. Phys.* **1986**, *84*, 4524.
[32] K. Eichkorn, O. Treutler, H. Ohm, M. Haser, R. Ahlrichs, *Chem. Phys. Lett.* **1995**, *242*, 652.
[33] K. Eichkorn, F. Weigend, O. Treutler, R. Ahlrichs, *Theor. Chem. Acc.* **1997**, *97*, 119.
[34] a) A. Schafer, H. Horn, R. Ahlrichs, *J. Chem. Phys.* **1992**, *97*, 2571; b) A. Schafer, C. Huber, R. Ahlrichs, *J. Chem. Phys.* **1994**, *100*, 5829.
[35] F. Neese, *J. Chem. Phys.* **2001**, *115*, 11080.
[36] J. P. Perdew, *Phys. Rev. B* **1986**, *34*, 7406.
[37] a) M. Romelt, S. Ye, F. Neese, *Inorg. Chem.* **2009**, *48*, 784; b) P. Jayapal, G. Rajaraman, *Phys. Chem. Chem. Phys.* **2012**, *14*, 9050.
[38] E. V. Lenthe, A. E. Ehlers, E. J. Baerends, *J. Chem. Phys.* **1999**, *110*, 8943.
[39] Relativistic regular two-component Hamiltonians: E. V. Lenthe, E. J. Baerends, J. G. Snijders, *J. Chem. Phys.* **1993**, *99*, 4597.
[40] a) A. D. Becke, *Phys. Rev. A* **1988**, *38*, 3098; b) J. P. Perdew, *Phys. Rev. B* **1986**, *33*, 8822; c) C. Lee, W. Yang, R. G. Parr, *Phys. Rev. B* **1988**, *37*, 785.
[41] Y. Zhao, D. G. Truhlar, *Theor. Chem. Acc.* **2008**, *120*, 215.
[42] *Molekel*, Advanced Interactive 3D-Graphics for Molecular Sciences; available under http:\\www.cscs.ch/molkel/; *Chemcraft*, version 1.6 (build 338), programming G. A. Zhurko; available under www.chemcraftprog.com.
[43] N. C. Handy, A. J. Cohen, *Mol. Phys.* **2000**, *99*, 403.
[44] a) M. Reiher, O. Salomon, B. A. Hess, *Theor. Chem. Acc.* **2001**, *107*, 48; b) O. Salomon, M. Reiher, B. A. Hess, *J. Chem. Phys.* **2001**, *117*, 4729; c) J. A. Wolny, H. Paulsen, J. J. McGarvey, R. Diller, V. Schunemann, H. Toftlund, *Phys. Chem. Chem. Phys.* **2009**, *11*, 7562.
[45] S. Miertus, E. Scrocco, J. Tomasi, *J. Chem. Phys.* **1981**, *55*, 117.
[46] a) M. A. Wong, M. J. Frisch, K. B. Wiberg, *J. Am. Chem. Soc.* **1991**, *113*, 4776; b) M. A. Wong, M. J. Frisch, K. B. Wiberg, *J. Am. Chem. Soc.* **1992**, *114*, 523.
[47] http://www.Gaussian.com/index.html.
[48] a) J. G. Kirkwood, *J. Chem. Phys.* **1934**, *2*, 767; b) J. G. Kirkwood, *J. Chem. Phys.* **1939**, *7*, 911; c) L. Onsager, *J. Am. Chem. Soc.* **1936**, *58*, 1486.
[49] K. Boguslawski, C. R. Jacob, M. Reiher, *J. Chem. Theory Comput.* **2011**, *7*, 2740.
[50] M. Atanasov, P. Comba, B. Martin, V. Muller, G. Rajaraman, H. Rohwer, S. Wunderlich, *J. Comput. Chem.* **2006**, *27*, 1263.
[51] K. P. Kepp, *Coord. Chem. Rev.* **2013**, *257*, 196.
[52] F. Neese, F. Wenmohs, A. Hensen, U. Becker, *Chem. Phys.* **2009**, *356*, 98.
[53] S. Grimme, *J. Chem. Phys.* **2006**, *124*, 34108.
[54] T. M. Ross, B. Moubaraki, D. R. Turner, G. J. Halder, G. Chastanet, S. M. Neville, J. D. Cashion, J.-F. Létard, S. R. Batten, K. S. Murray, *Eur. J. Inorg. Chem.* **2011**, *9*, 1395–1417.
[55] O. Kahn, *Molecular Magnetism*, VCH, Weinheim, **1993**.
[56] a) F. Neese, *Coord. Chem. Rev.* **2009**, *253*, 526; b) Y. Shengfa, F. Neese, *Inorg. Chem.* **2010**, *49*, 772; c) C. R. Jacob, M. Reiher, *Int. J. Quantum Chem.* **2012**, *112*, 3661; d) S. Zein, S. A. Borshch, *J. Am. Chem. Soc.* **2005**, *127*, 16197.
[57] H. Paulsen, L. Duelund, H. Winkler, H. Toftlund, A. X. Trautwein, *Inorg. Chem.* **2001**, *40*, 2201.
[58] H. Paulsen, A. Zimmermann, F. Averseng, M. Gerdan, H. Winkler, H. Toftlund, A. X. Trautwein, *Monatsh. Chem.* **2003**, *134*, 295.
[59] K. H. Hopmann, A. Ghosh, L. Noodleman, *Inorg. Chem.* **2009**, *48*, 9155.

Received: September 14, 2012
Published Online: January 18, 2013

